

Breaking and restoration of rotational symmetry for irreducible tensor operators on the lattice

Bing-Nan Lu,¹ Timo A. Lähde,¹ Dean Lee,² and Ulf-G. Meißner^{1,3,4}

¹*Institute for Advanced Simulation, Institut für Kernphysik, and Jülich Center for Hadron Physics, Forschungszentrum Jülich, D-52425 Jülich, Germany*

²*Department of Physics, North Carolina State University, Raleigh, North Carolina 27695, USA*

³*Helmholtz-Institut für Strahlen- und Kernphysik and Bethe Center for Theoretical Physics, Universität Bonn, D-53115 Bonn, Germany*

⁴*JARA-High Performance Computing, Forschungszentrum Jülich, D-52425 Jülich, Germany*

(Dated: 4-March-2015)

We study the breaking of rotational symmetry on the lattice for irreducible tensor operators and practical methods for suppressing this breaking. We illustrate the features of the general problem using an α cluster model for ${}^8\text{Be}$. We focus on the lowest states with non-zero angular momentum and examine the matrix elements of multipole moment operators. We show that the physical reduced matrix element is well reproduced by averaging over all possible orientations of the quantum state, and this is expressed as a sum of matrix elements weighted by the corresponding Clebsch-Gordan coefficients. For our α cluster model we find that the effects of rotational symmetry breaking can be largely eliminated for lattice spacings of $a \leq 1.7$ fm, and we expect similar improvement for actual lattice Monte Carlo calculations.

PACS numbers: 12.38.Gc, 03.65.Ge, 21.10.Dr

I. INTRODUCTION

In recent years, lattice Monte Carlo calculations have been widely applied to the study of nuclear structure [1–3]. In particular, chiral effective field theory (chiral EFT) combined with lattice methods has been employed to study the spectrum and structure of light and medium-mass nuclei [4–8]. In such calculations, continuous space-time is discretized and compactified so that path integrals can be computed numerically. The mesh points uniformly span a cubic box, and some boundary conditions such as periodic boundaries are imposed in each dimension. However, the calculated bound state energies and wave functions will, in general, deviate from their continuum infinite-volume counterparts due to the discretization and finite-volume artifacts.

Over the years, much effort has been devoted to removing numerical artifacts in lattice field theory calculations. The finite volume energy shifts for two-body bound states [9–18] as well as two-body resonances and scattering problems [19–23] have been studied in detail. There is also on-going research to extend these results to bound states with more than two constituents [12, 13, 24–28]. On the other hand, removing the artifacts from finite lattice spacing is a more complicated issue. For chiral EFT the lattice improvement program proposed by Symanzik *et al.* [29–31] provides a useful approach for systematically reducing discretization errors. This method was also applied to Yang-Mills theories [29, 30], gauge field theories [31–34] and QCD [35]. Dudek *et al.* [36] have proposed a method where the continuum spin of meson [37] and baryon [38, 39] excited states in lattice QCD can be reliably identified. Meanwhile, Davoudi *et al.* [40] have quantified the breaking and restoration of rotational invariance at both tree level and one-loop level by means of lattice operators smeared over a finite spatial region.

On the lattice, the full rotational symmetry group is reduced to the finite group of cubic rotations, $SO(3) \rightarrow SO(3, Z)$. Several basic rules based on the argument of rotational invariance are broken. For example, in the continuum and infinite-volume limits, quantum bound states with angular momentum J form a degenerate multiplet consisting of $2J + 1$ components, while on the lattice the energy levels split into subgroups corresponding to different irreducible representations (*irreps*) of the cubic group [41–43]. The size of the en-

ergy splittings are dictated by the lattice spacing and by the volume and boundary conditions.

In Ref. [44], we explored the breaking of rotational symmetry on the lattice for bound state energies with an α cluster model. It was shown that the calculated energy is minimized when the natural separation between particles is commensurate with the separation between lattice points along the preferred lattice directions associated with the given angular momentum state. It was also shown that the multiplet-averaged energy is closer to the continuum limit than any single energy level. One can apply these results to future *ab initio* lattice simulations for nuclear systems where α cluster structures are important.

In this paper, we extend the analysis of Ref. [44] to other observables besides the energy. One is often interested in the nuclear radii, quadrupole moments as well as transition probabilities. For example, an anomalously large radius compared with the usual $A^{1/3}$ scaling law is evidence for a halo nucleus [46, 47], while the intrinsic quadrupole moment is often related to the rotational bands observed in deformed nuclei [48].

We consider irreducible tensor operators sandwiched by a pair of bound state wave functions. In the continuum limit such an expression can be factorized and simplified according to the Wigner-Eckart theorem because of the full rotational symmetry, but on the lattice such factorization is no longer possible and the situation becomes more complicated. Furthermore, continuum selection rules for electromagnetic transitions are not exactly satisfied on the lattice. Some transitions that are absolutely forbidden by rotational symmetry may assume non-zero amplitudes on the lattice. We would like to construct proper corrections for these matrix elements in order to minimize symmetry breaking effects.

Our objective in this paper is to investigate anisotropic lattice artifacts in the matrix elements of irreducible tensor operators and search for a practical method to restore rotational symmetry. The details of the particular interaction are not essential to our general analysis. Here, we use the same α cluster model as in Ref. [44] where the α - α interaction is approximated by an Ali-Bodmer type potential adjusted to produce a bound ${}^8\text{Be}$ nucleus.

II. THEORETICAL FRAMEWORK

A. Hamiltonian

Let $m_\alpha = 3727.0$ MeV denote the mass of the α particle and $m = m_\alpha/2$ the reduced mass. Our starting point is the one-body Hamiltonian

$$H = -\frac{\nabla^2}{2m} + V(r), \quad (1)$$

where $r = \sqrt{x^2 + y^2 + z^2}$ is the distance between the two α particles, $V = V_N + V_C$ is the α - α potential, including nuclear and Coulomb potentials.

We use the same two-body potential as that used in Ref. [44]. For completeness we briefly introduce its functional form and the parameters. For the nuclear part of the α - α interaction we use an isotropic Ali-Bodmer-type potential,

$$V_N(r) = V_0 \exp(-\eta_0^2 r^2) + V_1 \exp(-\eta_1^2 r^2), \quad (2)$$

where $V_0 = -216.0$ MeV, $V_1 = 354.0$ MeV, $\eta_0 = 0.436$ fm $^{-1}$ and $\eta_1 = 0.529$ fm $^{-1}$. These parameters are determined by fixing the S - and D -wave α - α scattering lengths to their experimental values. The Coulomb potential is given by the error function

$$V_C(r) = \frac{4e^2}{r} \operatorname{erf}\left(\frac{\sqrt{3}r}{2R_\alpha}\right), \quad (3)$$

where $R_\alpha = 1.44$ fm is the radius of the α particle, e is the fundamental unit of charge and erf denotes the error function.

Since our focus is on measuring bound state properties and the physical ^8Be nucleus is unbound, we increase V_0 by an amount of 30%. With this strengthened potential, the ^8Be nucleus has a ground state at $E(0^+) = -10.8$ MeV and one excited state at $E(2^+) = -3.3$ MeV. These energies are measured relative to the α - α threshold.

In the lattice calculations the spatial vector \mathbf{r} assumes discrete values, and so the Hamiltonian in Eq. (1) becomes a matrix. Periodic boundary conditions for a box of size L are imposed on the wave functions,

$$\psi(\mathbf{r} + \mathbf{n}_i L) = \psi(\mathbf{r}), \quad (4)$$

where \mathbf{n}_i with $i = x, y, z$ are the unit vectors along the three coordinate axes. The energy eigenvalues and wave functions can be obtained by the diagonalization of the Hamiltonian matrix of dimension $L^{3(N-1)} \times L^{3(N-1)}$.

The kinetic energy term in Eq. (1) can be expressed on the lattice by finite differences. In one dimension we have

$$f''(x) \approx c_0^{(N)} f(x) + \sum_{k=1}^N c_k^{(N)} [f(x+ka) + f(x-ka)], \quad (5)$$

where a is the lattice spacing and $c_k^{(N)}$ is a set of fixed coefficients. The order- N formula involves $2N+1$ points and the corresponding truncation error is $\mathcal{O}(a^{2N})$. In Ref. [44], we gave the coefficients $c_k^{(N)}$ for $N \leq 4$. In this paper, we use the $N = 4$ formula to calculate the second-order derivatives appearing in the Laplace operator. This choice removes most of the rotational symmetry breaking effects due to the difference formula for the kinetic energy.

B. Lattice wave functions

The continuum Hamiltonian Eq. (1) is invariant under any spatial rotation. As a result, the bound states of H form angular momentum multiplets. Let us denote the bound state wave functions as ϕ_{lm} , where the integer l is the angular momentum and the integer m is the z -component of angular momentum with $-l \leq m \leq l$. For systems with more than one bound state with the same value of l , we will need additional radial quantum numbers. However, we do not consider such cases here. The angular dependence of these wave functions are given by the corresponding spherical harmonics Y_{lm} .

On the lattice, these angular momentum l multiplets are split into *irreps* of the cubic rotational group, $SO(3, Z)$. In Ref. [44], we gave the splitting patterns of the angular momentum multiplets with $l \leq 8$. In order to specify the wave functions belonging to the same *irrep*, we define a quantum number k that is valid on the lattice through the relation

$$R_z\left(\frac{\pi}{2}\right) = \exp\left(-i\frac{\pi}{2}k\right), \quad (6)$$

where $R_z(\pi/2)$ is a rotation around the z -axis by $\pi/2$. The integers k are equal to m modulo 4 and are non-degenerate for each *irrep* of O . We label the wave function $\psi_{l\tau k}$ for any eigenstate by l , k and the *irrep* τ it belongs to. If the angular momentum J contains more than one branch belonging to the same *irrep*, we distinguish them by adding primes to the name of the *irreps*. For instance, the symbol “ $\psi_{6T_2'1}$ ” denotes the wave function with $l = 6$, $k = 1$ belonging to the second T_2 *irrep*. Consequently, in the continuum limit the wave functions $\psi_{l\tau k}$ form a complete basis for the bound state subspace, and the corresponding energies are degenerate for the same total angular momentum J , while on the lattice the energy eigenvalue depends on both J and the *irrep* τ . In the continuum limit we can write down unitary transformations from the ϕ_{lm} basis to the $\psi_{l\tau k}$ basis and vice versa,

$$\phi_{lm} = \sum_{\tau k} U_{l\tau k} \psi_{l\tau k}, \quad (7)$$

$$\psi_{l\tau k} = \sum_m U_{l\tau k m}^{-1} \phi_{lm}. \quad (8)$$

See Ref. [45] for details of these transformations. As an example, we show the case of $l = 2$. The wave functions ψ_{2E0} , ψ_{2E2} belong to *irrep* E , and $\psi_{2T_2'1}$, $\psi_{2T_2'2}$, $\psi_{2T_2'3}$ belong to *irrep* T_2 . Following Ref. [45] we find

$$\begin{aligned} \psi_{2E0} &= \phi_{20}, & \psi_{2T_2'1} &= \phi_{21}, & \psi_{2T_2'3} &= \phi_{2\bar{1}}, \\ \psi_{2E2} &= \sqrt{\frac{1}{2}}(\phi_{22} + \phi_{2\bar{2}}) & \psi_{2T_2'2} &= -i\sqrt{\frac{1}{2}}(\phi_{22} - \phi_{2\bar{2}}). \end{aligned} \quad (9)$$

We write \bar{m} for notational convenience to denote $-m$.

On the lattice we can obtain the bound state wave functions $\psi_{l\tau k}$ by simultaneously diagonalizing the lattice Hamiltonian H (or transfer matrix [1]) and the $R_z(\pi/2)$ operator. Since the full rotational symmetry is broken, the angular momentum l should be viewed as a label that describes the angular momentum multiplet obtained by dialing the lattice spacing continuously to zero. But we can use the unitary transformation in Eq. (7) to define the wavefunctions ϕ_{lm} at non-zero lattice spacing. We do this even though the wavefunctions ϕ_{lm} are generally not exact eigenstates of H when the lattice spacing is non-zero.

Consider now the bound state wavefunctions for a zero angular momentum state ϕ_{00} and a general state ϕ_{lm} . In the continuum limit the matrix elements of a $r^l Y_{lm}$ multipole operator inserted between ϕ_{00} and ϕ_{lm} must be independent of m ,

$$\begin{aligned} & \langle \phi_{lm} | r^l Y_{lm} | \phi_{00} \rangle \\ & \equiv \int d^3 \mathbf{r} \langle \phi_{lm} | \rho(\mathbf{r}) r^l Y_{lm}(\Omega) | \phi_{00} \rangle = C_m \rightarrow C. \end{aligned} \quad (10)$$

When using Eq. (7), we find the condition that C_m is independent of m a very convenient check that the phases for ϕ_{lm} and $\psi_{l\tau k}$ are consistent with standard conventions as defined in Ref. [45].

C. Factorization of the matrix elements

Given a pair of bound state wave functions $\phi_{l_1 m_1}(\mathbf{r})$ and $\phi_{l_2 m_2}(\mathbf{r})$ with angular momenta l_1, m_1, l_2 and m_2 on the lattice, we can evaluate the matrix element of the multipole moment operator $r^l Y_{lm}$,

$$\langle l_1 m_1 | r^l Y_{lm} | l_2 m_2 \rangle = \sum_{\mathbf{n}} \phi_{l_1 m_1}^*(\mathbf{n}a) |\mathbf{n}a|^l Y_{lm}(\hat{\mathbf{n}}) \phi_{l_2 m_2}(\mathbf{n}a), \quad (11)$$

where \mathbf{n} runs over all lattice sites. Here, we choose independent integers l and l' in the multipole moment operator, in order to keep the radial and angular degrees of freedom independent. This makes our conclusions sufficiently general and applicable to all irreducible tensor operators. We use parentheses to denote matrix elements on the lattice, $\langle f | O | i \rangle$, and Dirac brackets to denote matrix elements in the continuum limit, $\langle f | O | i \rangle$. The continuum limit of Eq. (11) is

$$\langle l_1 m_1 | r^l Y_{lm} | l_2 m_2 \rangle = \int d^3 \mathbf{r} \phi_{l_1 m_1}^*(\mathbf{r}) r^l Y_{lm}(\Omega) \phi_{l_2 m_2}(\mathbf{r}) \quad (12)$$

where the integration is performed over all space. Matrix elements in the form of Eq. (12) occur frequently in the calculation of various nuclear observables such as the mean square radii, quadrupole moments, transition probabilities, *etc.* Here we focus on lattice artifacts that produce some residual difference between the values in Eq. (11) and Eq. (12) and the methods for removing them.

Let us start with the continuum limit. According to the Wigner-Eckart theorem, the matrix element (12) can be transformed into a product of two factors: Clebsch-Gordan (C-G) coefficients and the reduced matrix element that contains the essential non-trivial physics. Let $R_1(r)$ and $R_2(r)$ be the radial parts of the wave functions $\phi_{l_1 m_1}(\mathbf{r})$ and $\phi_{l_2 m_2}(\mathbf{r})$, respectively, so that

$$\langle l_1 m_1 | r^l Y_{lm} | l_2 m_2 \rangle = \langle l_1 | r^l | l_2 \rangle \mathcal{Q}_{l_2 m_2, l m}^{l_1 m_1}, \quad (13)$$

where

$$\langle l_1 | r^l | l_2 \rangle = \int dr r^{l'+2} R_1^*(r) R_2(r) \quad (14)$$

$$\mathcal{Q}_{l_2 m_2, l m}^{l_1 m_1} = \int d\Omega Y_{l_1 m_1}^*(\Omega) Y_{lm}(\Omega) Y_{l_2 m_2}(\Omega). \quad (15)$$

The radial integral in Eq. (14) is the matrix element of the l' -order moment operator r^l and is independent of the quantum numbers m_1, m and m_2 . Meanwhile $\mathcal{Q}_{l_2 m_2, l m}^{l_1 m_1}$ can be written as a product of C-G coefficients,

$$\mathcal{Q}_{l_2 m_2, l m}^{l_1 m_1} = \sqrt{\frac{(2l+1)(2l_2+1)}{4\pi(2l_1+1)}} C_{l_2 0, l 0}^{l_1 0} C_{l_2 m_2, l m}^{l_1 m_1} \quad (16)$$

All of the dependence on the quantum numbers m_1, m, m_2 and l is absorbed into $\mathcal{Q}_{l_2 m_2, l m}^{l_1 m_1}$. Instead of simply factoring out the C-G coefficient $C_{l_2 m_2, l m}^{l_1 m_1}$, we find this factorization useful because the radial integrals of r^l are physically meaningful. In Table I, we list some factors $\mathcal{Q}_{l_2 m_2, l m}^{l_1 m_1}$ with $l_1 = l_2 = 2$ and l from 0 to 4. The other factors can be obtained from standard tables of C-G coefficients.

Since full rotational symmetry is broken on the lattice, it is not possible to write the wave functions as products of radial and angular parts. However, one can still apply the Wigner-Eckart theorem to each *irrep* of the cubic group. As a result, the matrix elements calculated on the lattice belonging to the same *irreps* are related by C-G coefficients of the cubic group, which can be computed easily using decompositions into spherical harmonics [45, 49]. For example, we have

$$(2T_2 1 | r^2 Y_{2E0} | 2T_2 1) = -\sqrt{\frac{1}{3}} (2T_2 1 | r^2 Y_{2E2} | 2T_2 \bar{1}), \quad (17)$$

where Y_{2E0} and Y_{2E2} are defined as

$$Y_{2E0} = Y_{20}, \quad Y_{2E2} = \sqrt{\frac{1}{2}} (Y_{22} + Y_{\bar{2}2}), \quad (18)$$

in analogy to the relations in Eq. (9). The ratio of $-\sqrt{1/3}$ is irrespective of the lattice spacing, box size or the strength of the interaction.

We will divide the lattice matrix elements in Eq. (11) by the $\mathcal{Q}_{l_2 m_2, l m}^{l_1 m_1}$ as defined in Eq. (16) whenever non-zero, even though the factorization in Eq. (13) is not exact on the lattice. We represent the resulting quantity by double vertical lines,

$$\langle l_1 m_1 || r^l Y_{lm} || l_2 m_2 \rangle = \langle l_1 m_1 | r^l Y_{lm} | l_2 m_2 \rangle / \mathcal{Q}_{l_2 m_2, l m}^{l_1 m_1}, \quad (19)$$

for $\mathcal{Q}_{l_2 m_2, l m}^{l_1 m_1} \neq 0$. It is clear that these reduced matrix elements all converge to the radial matrix element $\langle l_1 | r^l | l_2 \rangle$ as $a \rightarrow 0$. At non-zero lattice spacing, however, the ratio will depend on the quantum numbers m_1, m_2 and m . Therefore, the splittings between different components of Eq. (19) are sensitive indicators of the rotational symmetry breaking effects.

D. Isotropic average

We now focus on spatial anisotropies which are associated with the orientation of our lattice wave functions ϕ_{lm} relative to the lattice axes. Let us illustrate this point by recalculating the matrix element $\langle l_1 m_1 | r^l Y_{lm} | l_2 m_2 \rangle$ with a tilted lattice which differs from the original one by a rigid body rotation. Let us assume that the wave functions $\phi_{l_1 m_1}$ and $\phi_{l_2 m_2}$ can be smoothly interpolated in between lattice points as a function in continuous space. Then we can define a tilted matrix element as

$$\begin{aligned} & \langle l_1 m_1 | r^l Y_{lm} | l_2 m_2 \rangle_{\Lambda} \\ & = \sum_{\mathbf{n}} \phi_{l_1 m_1}^*(R(\Lambda) \mathbf{n}a) |\mathbf{n}a|^l Y_{lm}(R(\Lambda) \hat{\mathbf{n}}) \phi_{l_2 m_2}(R(\Lambda) \mathbf{n}a), \end{aligned} \quad (20)$$

where $\Lambda = (\alpha, \beta, \gamma)$ is a set of Euler angles and $R(\Lambda)$ is an element of the SO(3) rotation group. In the continuum limit, rotational invariance guarantees that $\langle l_1 m_1 | r^l Y_{lm} | l_2 m_2 \rangle$ and $\langle l_1 m_1 | r^l Y_{lm} | l_2 m_2 \rangle_{\Lambda}$

l_1	l	l_2	m_1	m	m_2	$Q_{l_2 m_2, l m}^{l_1 m_1}$	m_1	m	m_2	$Q_{l_2 m_2, l m}^{l_1 m_1}$
2	0	2	0	0	0	$\frac{1}{2\sqrt{\pi}}$	1	0	1	$\frac{1}{2\sqrt{\pi}}$
			2	0	2	$\frac{1}{2\sqrt{\pi}}$				
2	2	2	0	0	0	$\frac{1}{7}\sqrt{\frac{5}{\pi}}$	2	1	1	$\sqrt{\frac{15}{14\pi}}$
			2	0	2	$-\frac{1}{7}\sqrt{\frac{5}{\pi}}$	1	1	0	$\frac{1}{14}\sqrt{\frac{5}{\pi}}$
			2	2	0	$-\frac{1}{7}\sqrt{\frac{5}{\pi}}$	1	0	1	$\frac{1}{14}\sqrt{\frac{5}{\pi}}$
			1	2	$\bar{1}$	$-\sqrt{\frac{15}{14\pi}}$				
2	4	2	0	0	0	$\frac{3}{7\sqrt{\pi}}$	1	3	$\bar{2}$	$\frac{1}{2}\sqrt{\frac{5}{7\pi}}$
			2	0	2	$\frac{1}{14\sqrt{\pi}}$	1	2	$\bar{1}$	$-\frac{1}{7}\sqrt{\frac{10}{\pi}}$
			2	1	1	$-\frac{1}{14}\sqrt{\frac{5}{\pi}}$	1	0	1	$-\frac{2}{7\sqrt{\pi}}$
			1	1	0	$\frac{1}{7}\sqrt{\frac{15}{2\pi}}$	2	2	0	$\frac{1}{14}\sqrt{\frac{15}{\pi}}$
			2	4	$\bar{2}$	$\sqrt{\frac{5}{14\pi}}$				

Table I. The factor $Q_{l_2 m_2, l m}^{l_1 m_1}$ defined in Eq. (16) with $l_1 = l_2 = 2$ and l from 0 to 4. The other ratios not listed here can be obtained from standard tables of C-G coefficients.

are equal. For non-zero lattice spacing and non-zero angular momenta, however, the tilted matrix element will depend on the quantity Λ . We would like to eliminate this unphysical orientation dependence from the final results.

A natural choice is to average the results over all possible orientations, or equivalently, over the whole SO(3) group space. The isotropically-averaged matrix element is defined as

$$(l_1 m_1 | r^{l'} Y_{lm} | l_2 m_2)_\circ = \int d^3 \Lambda (l_1 m_1 | r^{l'} Y_{lm} | l_2 m_2)_\Lambda$$

$$= C_{l_2 m_2, l m}^{l_1 m_1} \left[\frac{1}{2l_1 + 1} \sum_{m', m'_1, m'_2} C_{l_2 m'_2, l m'}^{l_1 m'_1} (l_1 m'_1 | r^{l'} Y_{lm'} | l_2 m'_2) \right]. \quad (21)$$

Here, $d^3 \Lambda$ is the normalized invariant measure on the SO(3) group space and the subscript “ \circ ” denotes the isotropic average. In analogy with Eq. (19), it is convenient to define a reduced isotropically-averaged matrix element,

$$(l_1 || r^{l'} Y_l || l_2)_\circ = (l_1 m_1 | r^{l'} Y_{lm} | l_2 m_2)_\circ / Q_{l_2 m_2, l m}^{l_1 m_1} \quad (22)$$

for $Q_{l_2 m_2, l m}^{l_1 m_1} \neq 0$. In the continuum limit $(l_1 || r^{l'} Y_l || l_2)_\circ$ coincides with the radial matrix element $\langle l_1 | r^{l'} | l_2 \rangle$.

We note that the radial matrix element $\langle l_1 | r^{l'} | l_2 \rangle$ is not only independent of m , m_1 and m_2 , but also independent of l . So a non-trivial test of rotational symmetry restoration is to check that $(l_1 || r^{l'} Y_l || l_2)_\circ$ as defined in Eq. (22) is independent of l . If $(l_1 || r^{l'} Y_l || l_2)_\circ$ is to a good approximation independent of l , then we have succeeded in approximately factorizing the radial and angular parts of the lattice wave function by means of isotropic averaging. We will test this numerically with the α cluster model in Sec. III.

III. RESULTS

We start with the mean square radius operator r^2 . This corresponds to setting $l = 0$ and $l' = 2$ in Eq. (11) and Eq. (12). In the upper panel of Fig. 1, we show the expectation values of r^2 for the lowest 2^+ states as functions of the lattice spacing a . The eigenstate wave functions $\psi_{2\tau k}$ are obtained by simultaneously diagonalizing the Hamiltonian H in Eq. (1) and the $R_z(\pi/2)$ operator. We then construct the linear combinations ϕ_{2m} according to Eq. (9). We write $(m || 0 || m)$ as an abbreviation for $(2m || r^2 Y_{00} || 2m)$ and the solid curve denotes the isotropic average $(2 || r^2 Y_{00} || 2)_\circ$ defined in Eq. (22). Only three values with $m \geq 0$ are shown since time reversal symmetry ensures equal results for m and $-m$. As discussed in Sec. II, all these reduced matrix elements converge to $\langle r^2 \rangle \equiv \langle l_1 = 2 | r^2 | l_2 = 2 \rangle$ as $a \rightarrow 0$. Note that in all the following calculations, we remove the finite volume effects by using a box size of $L \geq 16$ fm.

The three branches are not linearly independent because of the cubic symmetries on the lattice. For scalar operators, the linear relations among them are manifest. According to Eq. (9), the wave functions ϕ_{21} and ϕ_{20} belong to the *irreps* E and T_2 , respectively. Meanwhile the wave function ϕ_{22} is a mixture of the *irreps* E and T_2 with equal weights. Thus, $(2 || 0 || 2)$ equals the arithmetic average of $(0 || 0 || 0)$ from *irrep* E and $(1 || 0 || 1)$ from *irrep* T_2 . So we find that the isotropically-averaged reduced matrix element $(2 || r^2 Y_0 || 2)_\circ$ is given by

$$(2 || r^2 Y_0 || 2)_\circ = \frac{3}{5} (1 || 0 || 1) + \frac{2}{5} (0 || 0 || 0), \quad (23)$$

where the numerators 3 and 2 are simply the dimensions of each cubic representation. It is easy to verify that the weighted average formula is applicable for any angular momentum with the factors 3 and 2 in Eq. (23) replaced by the corresponding *irrep* dimensions. In Ref. [44] we introduced the multiplet-weighted average to eliminate the anisotropic effects in the bound state energies. We have now proven that this procedure is equivalent to averaging over lattice orientations and applies to the expectation value of any scalar operator.

Next, let us examine the dependence of these reduced matrix elements on the lattice spacing a . For $a \leq 1.0$ fm, the three branches merge, and for large a they split and show oscillations. Before discussing the details and the physics behind them, it is interesting to compare Fig. 1 in this paper to Fig. 3 in Ref. [44] where the calculated 2^+ energies are shown as functions of a . We immediately find that these figures look similar if we map $(1 || 0 || 1)$ to $E(2^+_{\bar{1}})$, and $(0 || 0 || 0)$ to $E(2^+_{\bar{2}})$. More specifically, in Fig. 1 the splitting between the two branches has two zeros near $a = 1.4$ fm and 1.9 fm. For $a \leq 1.0$ fm, the splitting is negligible. For $1.0 \leq a \leq 1.4$ fm, $(1 || 0 || 1)$ is higher than $(0 || 0 || 0)$. However, in the region $1.4 \leq a \leq 1.9$ fm, the order is reversed. For $a \geq 1.9$ fm, $(1 || 0 || 1)$ is once again higher and the splitting increases monotonically. This behavior also occurs for the energies in Ref. [44] with slightly different turning points. Additionally, the weighted averages $(2 || r^2 Y_0 || 2)_\circ$ and $E(2^+_{\bar{A}})$ both show down bending in the transitional region $1.5 \leq a \leq 2.0$ fm, resulting in smaller expectation values for both energy and radii at large lattice spacings.

The same pattern is also observed for other scalar operators. In the lower panel of Fig. 1, we show the results for the r^4 operator which corresponds to setting $l = 0$ and $l' = 4$. Here, the symbols $(m || 0 || m)$ are abbreviations of $(2m || r^4 Y_{00} || 2m)$ and the solid curve

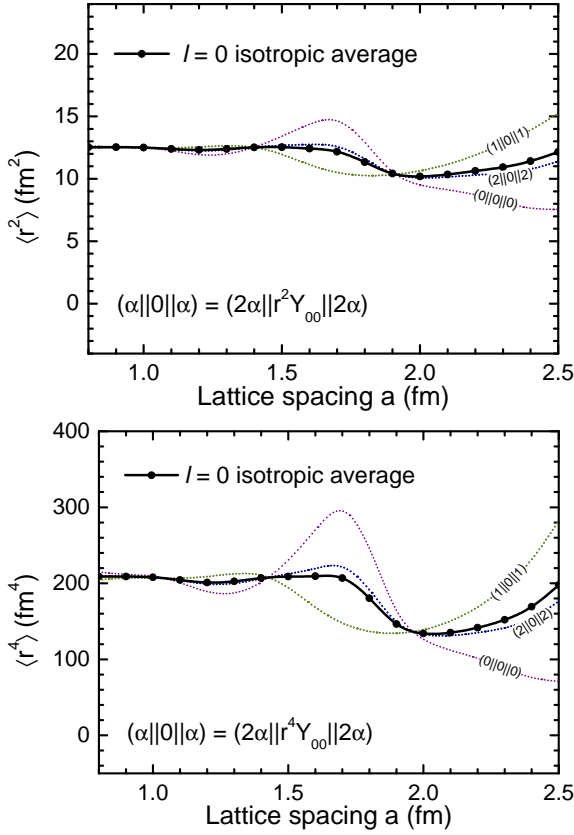


Figure 1. (color online). *Upper panel:* Mean square radii $\langle r^2 \rangle$ for the lowest 2^+ states of the ${}^8\text{Be}$ nucleus as a function of a . $(\alpha||0||\alpha)$ is an abbreviation of the reduced lattice matrix element $(2\alpha||r^2Y_{00}||2\alpha)$ defined in Eq. (19), which converges to $\langle r^2 \rangle$ as $a \rightarrow 0$. The box size L is kept larger than 16 fm to remove finite volume effects. The solid line represents the isotropic average $(2||r^2Y_0||2)_\circ$ defined in Eq. (22). *Lower panel:* Mean value $\langle r^4 \rangle$ for the lowest 2^+ states of the ${}^8\text{Be}$ nucleus as a function of a . $(\alpha||0||\alpha)$ is an abbreviation of the reduced lattice matrix element $(2\alpha||r^4Y_{00}||2\alpha)$, which converges to $\langle r^4 \rangle$ as $a \rightarrow 0$. The solid line represents the isotropic average $(2||r^4Y_0||2)_\circ$.

denotes the isotropic average. All curves converge to the expectation value $\langle r^4 \rangle \equiv \langle l_1 = 2 | r^4 | l_2 = 2 \rangle$ as $a \rightarrow 0$. Again, the isotropic average is just the multiplet-weighted average over the five-fold multiplet ϕ_{2m} . Apparently, the oscillations of these components as well as the down bending of the isotropic average are quite similar to the ones observed for the r^2 operator.

Based on the results shown in Fig. 1, we can compare the various components $(m||0||m)$ to the continuum limit and select the ones with the least lattice spacing dependence. It seems that $(1||0||1)$ and $(0||0||0)$ are not optimal for both r^2 and r^4 operators because of their large deviations from the continuum values for sparse lattices. The arithmetical average $(2||0||2)$ and the multiplet-weighted average are close to each other for all lattice spacings considered here. In principle, both of them can be used as a good approximation to the continuum limit. Nevertheless, the multiplet-weighted average is theoretically preferable because of its clear physical interpretation as isotropic averaging.

Our conclusions for the operators r^2 , r^4 as well as the energy can be generalized straightforwardly to other scalar operators on the lattice. For example, the linear relation among the components

$(0||0||0)$, $(1||0||1)$ and $(2||0||2)$ is also satisfied there. In order to estimate the continuum value, we can calculate the isotropic average according to Eq. (22) which equals the weighted average over the angular momentum multiplet in the case of scalar operators.

We now turn to the case of $l = 2$. In the upper panel of Fig. 2, the symbols $(\alpha||\beta||\gamma)$ are abbreviations of the reduced matrix elements $(2\alpha||r^2Y_{2\beta}||2\gamma)$ defined in Eq. (19), where the subscripts α , β and γ run from -2 to 2 and only the components with $\alpha = \beta + \gamma$ are shown. The solid curve represents the isotropic average defined in Eq. (22). All these curves converge to the mean square radius $\langle r^2 \rangle$ as $a \rightarrow 0$. Note that while the $2J + 1$ wave functions in an angular momentum multiplet are mixed with each other on the lattice, some components with $\alpha \neq \beta + \gamma$ survive for large lattice spacings. However, because the corresponding C-G coefficients vanish in this case, these components do not contribute to the isotropic average.

Compared to the case of the scalar operator r^2 shown in Fig. 1, the insertion of the spherical harmonic $Y_{2\beta}$ makes Fig. 2 much more complicated. Nevertheless, we can still draw some general conclusions. First, as for the scalar operators, we can show that $(2||0||2)$ is just the arithmetical average of $(1||0||1)$ and $(0||0||0)$, while $(2||2||0)$ is just the arithmetical average of $(1||1||0)$ and $(0||0||0)$. This point is apparent in Fig. 2, if we notice that in each group the three curves intersect at one point. Second, applying the Wigner-Eckart theorem for the cubic group, we can write several linear identities consisting of the lattice matrix elements. They concern not only the components shown in Fig. 2 but also the one that vanish as $a \rightarrow 0$.

In the upper panel of Fig. 2, most of the components show oscillations and have more than one extremum in this region. For example, $(0||0||0)$ reaches a maximum at $a = 1.6$ fm and two minima at $a = 1.2$ fm and 2.1 fm, respectively, while the $(1||0||1)$ only has an apparent minimum at $a = 1.8$ fm. For large lattice spacings, the calculated values usually deviate from the continuum ones by 50% to 100%. If we want to approximate the continuum limit using a single component in the lattice calculations, $(2||1||1)$ is the best choice. The corresponding curve only deviates slightly from the continuum value 12.5 fm² when $a > 2.0$ fm, which is sufficient for most recent lattice simulations of nuclei.

An anomaly occurs at $a = 2.1$ fm where the calculated matrix element $(0||0||0)$ becomes negative, whereas the continuum limit is a definitely positive number $\langle r^2 \rangle$. This discrepancy arises because we do not calculate the expectation value of the operator r^2 with the same wave functions on both sides, as was the case for scalar operators as shown in Fig. 1. For the $l = 2$ matrix elements in Fig. 2, the reduced matrix element $(0||0||0)$ is defined to be proportional to the expectation value of the quadrupole operator r^2Y_{20} . On the lattice the angular part of the quadrupole operator can not be separated completely, thus the insertion of the spherical harmonic Y_{20} is not fully canceled by the C-G coefficients included in Eq. (19). The remaining lattice artifacts may become as large as the magnitude of the observable itself. Therefore, it is dangerous to use randomly selected matrix elements calculated at large a as approximations of the continuum results, otherwise we may even find vanishing results for certain lattice spacings, which is unrealistic.

In spite of the diversity of the behaviors of the various components, we can eliminate the anisotropy of the lattice artifacts by calculating the isotropic average according to Eq. (22). In the upper panel of Fig. 2, the isotropic average as a function of the lattice spacing is represented by the solid line. In this case, the expression can not be written as a simple multiplet-weighted average

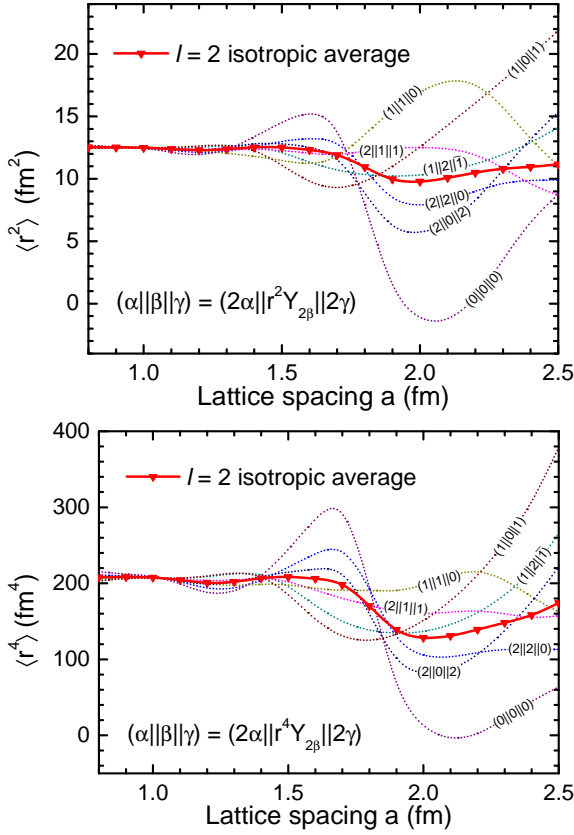


Figure 2. (color online). *Upper panel*: Mean square radii $\langle r^2 \rangle$ for the lowest 2^+ states of the ${}^8\text{Be}$ nucleus as a function of a . $(\alpha||\beta||\gamma)$ is an abbreviation of the reduced lattice matrix element $(2\alpha||r^2Y_{2\beta}||2\gamma)$ defined in Eq. (19), which converges to $\langle r^2 \rangle$ as $a \rightarrow 0$. The solid line represents the isotropic average $(2||r^2Y_2||2)_\circ$ defined in Eq. (22). *Lower panel*: Mean value $\langle r^4 \rangle$ for the lowest 2^+ states of the ${}^8\text{Be}$ nucleus as a function of a . $(\alpha||\beta||\gamma)$ is an abbreviation of the reduced lattice matrix element $(2\alpha||r^4Y_{2\beta}||2\gamma)$, which converges to $\langle r^4 \rangle$ as $a \rightarrow 0$. The solid line represents the isotropic average $(2||r^4Y_2||2)_\circ$.

because the C-G coefficients are no longer all the same. Similar to the isotropic average shown in the upper panel of Fig. 1, the isotropic average in Fig. 2 curve slightly bends downward in the region $1.5 \text{ fm} \leq a \leq 2.0 \text{ fm}$. For the lattice spacings considered here, the range of values obtained are between 9.8 fm^2 and 12.5 fm^2 , accounting for a 20% relative error with respect to the continuum limit. The component that is closest to the isotropic average for all lattice spacings is $(1||2||\bar{1})$.

Now let us change the radial factor of the inserted operator and keep the angular part the same. In the lower panel of Fig. 2, the symbol $(\alpha||\beta||\gamma)$ denotes the lattice reduced matrix element $(2\alpha||r^4Y_{2\beta}||2\gamma)$ which converges to $\langle r^4 \rangle$ as $a \rightarrow 0$. The solid line represents the isotropic average $(2||r^4Y_2||2)_\circ$. Again the inserted spherical harmonic $Y_{2\beta}$ is not fully canceled by the C-G coefficients on the lattice. The remaining lattice artifacts shift the various components from the continuum limit by different amounts for large lattice spacings. Nevertheless, comparing the curves denoted by the same symbol in the upper and lower panel of Fig. 2, we find that their behavior is *qualitatively* similar. For example, the $(0||0||0)$ curves both show a maximum at $a = 1.6 \text{ fm}$ and a minimum at 2.1

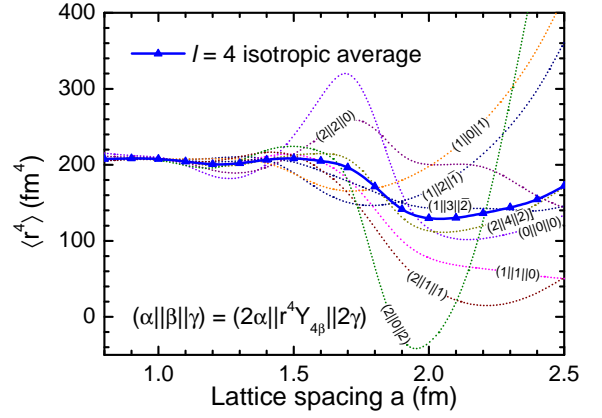


Figure 3. (color online) Mean value $\langle r^4 \rangle$ for the lowest 2^+ states of the ${}^8\text{Be}$ nucleus as a function of a . $(\alpha||\beta||\gamma)$ is an abbreviation of the reduced lattice matrix element $(2\alpha||r^4Y_{4\beta}||2\gamma)$ defined in Eq. (19), which converges to $\langle r^4 \rangle$ as $a \rightarrow 0$. The solid line represents the isotropic average $(2||r^4Y_4||2)_\circ$ defined in Eq. (22).

fm, while the $(2||0||2)$ curves both show a minimum at 2.0 fm . In other words, the magnitude of the lattice artifacts may be different if the radial part of the inserted operator is changed, but the pattern of oscillations and the sign of the deviations are largely determined by the angular momenta of the states and the irreducible tensor operator.

Next, we turn to the irreducible tensor operators with $l = 4$. In Fig. 3 the symbol $(\alpha||\beta||\gamma)$ denotes the lattice reduce matrix element $(2\alpha||r^4Y_{4\beta}||2\gamma)$ which converges to $\langle r^4 \rangle$ as $a \rightarrow 0$. The solid line represents the isotropic average $(2||r^4Y_4||2)_\circ$. Now the number of independent components is larger than that in the case of $l = 2$ and the situation is different. For example, the $(0||0||0)$ curve is much closer to the isotropic average compared to the corresponding curve in the lower panel of Fig. 2, while the $(2||0||2)$ curve has a pronounced minimum at $a = 2.0 \text{ fm}$. The component closest to the continuum limit as well as the isotropic average for all lattice spacings considered here is $(1||3||\bar{2})$. There also exist a number of linear relations among these components, which is a consequence of the remaining unbroken symmetry group. There is also a negative component $(2||0||2)$ at $a = 2.0 \text{ fm}$. We will not discuss all the details because most of them are natural extensions of the $l = 2$ case.

Finally, let us examine the postulate that the anisotropy resulting from the lattice artifacts is removed in the isotropic average, Eq. (22). In the upper panel of Fig. 4 we show the comparison between the isotropic averages $(2||r^2Y_0||2)_\circ$ and $(2||r^2Y_2||2)_\circ$. The former one is calculated with a simple multiplet averaging over the five fold branches, while the latter one is obtained by a relatively complicated averaging with the C-G coefficients as the weights. Clearly, for all the lattice spacings considered here, the difference between the two curves is rather small. Especially, the down bending occurs for the same lattice spacing and the magnitudes are also similar. Remembering that the C-G coefficients are included explicitly in the definition of isotropic average Eq. (22), we conclude that the effect of the angular part of the inserted operators is canceled by the C-G coefficients in the nominator. As is discussed in the previous section, this is a strong evidence for approximate rotational symmetry restoration and that we have factorized the radial and angular parts

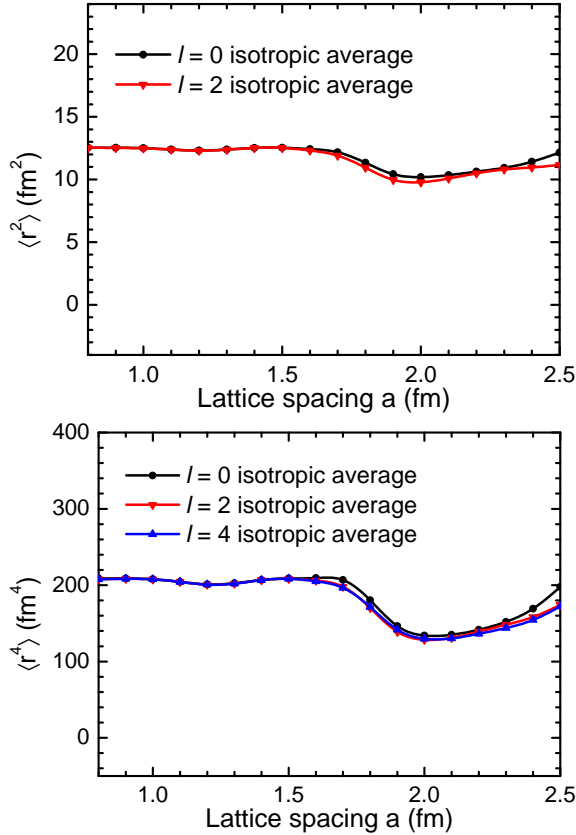


Figure 4. (Color online) *Upper panel*: Mean square radii $\langle r^2 \rangle$ for the lowest 2^+ states of the ${}^8\text{Be}$ nucleus as a function of a . The black and red lines represent the isotropic average $(2\|r^2Y_0\|2)_\circ$ and $(2\|r^2Y_2\|2)_\circ$, respectively. *Lower panel*: Expectation value $\langle r^4 \rangle$ for the lowest 2^+ states of the ${}^8\text{Be}$ nucleus as a function of a . The black, red and blue lines represent the isotropic averages $(2\|r^4Y_0\|2)_\circ$, $(2\|r^4Y_2\|2)_\circ$ and $(2\|r^4Y_4\|2)_\circ$, respectively.

of the lattice wave function by means of isotropic averaging.

In the lower panel of Fig. 4 we show the quantities that converge to $\langle r^4 \rangle$ as $a \rightarrow 0$, including $(2\|r^4Y_0\|2)_\circ$, $(2\|r^4Y_2\|2)_\circ$ and $(2\|r^4Y_4\|2)_\circ$. The three curves coincide with each other even for $a > 2.0$ fm, which means that the rotational symmetry is restored to a large extent after the isotropic averaging. In particular, the difference between the $l = 2$ and $l = 4$ results is almost zero for all the lattice spacings.

IV. SUMMARY

In lattice calculations, discretization errors can break rotational symmetry. The degeneracy of bound state multiplets with the same

angular momentum is broken on the lattice. The resulting wave functions are classified according to the irreducible representations of the cubic group instead of the full $\text{SO}(3)$ rotational group. For most of the observables represented by the irreducible tensor operators, the relations between the various components become complicated. In this paper, we used an α cluster model to investigate the lattice matrix elements of such operators. We have shown that the qualitative behaviors of the various matrix elements versus lattice spacing is mainly determined by the angular momenta of the states and operators. The matrix elements of different operators with the same angular momentum show a similar behavior as functions of the lattice spacing.

We have also defined an isotropic average in which the various components of the matrix element are linearly combined. The weight for a component is proportional to the corresponding C-G coefficients with the same quantum numbers. We have shown that such a calculation is equivalent to averaging over all possible lattice orientations. In such a calculation, we eliminate to a good approximation the anisotropy of the lattice artifacts. This point is illustrated by numerical calculations for the ${}^8\text{Be}$ nucleus with the α cluster model.

We have calculated the isotropic averages as functions of the lattice spacing for irreducible tensor operators with different angular momenta and same radial factors and find good agreement with continuum limit values. Comparing the results calculated with different lattice spacings, we found that there is a down bending of $\langle r^2 \rangle$ and $\langle r^4 \rangle$ in the region $1.7 \text{ fm} \leq a \leq 2.0 \text{ fm}$. For $a < 1.7 \text{ fm}$, the lattice artifacts are very small.

Although all the conclusions in this paper are obtained with a simple α cluster model, the results can be applied immediately to *ab initio* lattice simulations as well. For example, when calculating the transition amplitude between low-energy excited states and the ground state of a nucleus, we can improve the results by calculating the isotropic average to eliminate rotational symmetry breaking effects on the lattice.

ACKNOWLEDGMENTS

We acknowledge partial financial support from the Deutsche Forschungsgemeinschaft (Sino-German CRC 110), the Helmholtz Association (Contract No. VH-VI-417), BMBF (Grant No. 05P12PDTEE), the U.S. Department of Energy (DE-FG02-03ER41260), by the EU HadronPhysics3 project and the Magnus Ehrnrooth Foundation of the Finnish Society of Sciences and Letters.

-
- [1] D. Lee, *Prog. Part. Nucl. Phys.* **63**, 117 (2009).
 [2] A. Bazavov, D. Toussaint, C. Bernard, J. Laiho, C. DeTar, L. Levkova, M. B. Oktay, S. Gottlieb, U. M. Heller, J. E. Hetrick, P. B. Mackenzie, R. Sugar, and R. S. Van de Water, *Rev. Mod. Phys.* **82**, 1349 (2010).
 [3] S. Beane, W. Detmold, K. Orginos, and M. Savage, *Prog. Part. Nucl. Phys.* **66**, 1 (2011).

- [4] B. Borasoy, E. Epelbaum, H. Krebs, D. Lee, and U.-G. Meißner, *Eur. Phys. J. A* **31**, 105 (2007).
 [5] E. Epelbaum, H. Krebs, D. Lee, and U.-G. Meißner, *Eur. Phys. J. A* **45**, 335 (2010).
 [6] E. Epelbaum, H. Krebs, D. Lee, and U.-G. Meißner, *Phys. Rev. Lett.* **104**, 142501 (2010).

- [7] E. Epelbaum, H. Krebs, D. Lee, and U.-G. Meißner, *Phys. Rev. Lett.* **106**, 192501 (2011).
- [8] E. Epelbaum, H. Krebs, T. A. Lähde, D. Lee, and U.-G. Meißner, *Phys. Rev. Lett.* **110**, 112502 (2013).
- [9] M. Lüscher, *Comm. Math. Phys.* **104**, 177 (1986).
- [10] M. Lüscher, *Nucl. Phys. B* **354**, 531 (1991).
- [11] S. Beane, P. Bedaque, A. Parreño, and M. Savage, *Phys. Lett. B* **585**, 106 (2004).
- [12] S. König, D. Lee, and H.-W. Hammer, *Phys. Rev. Lett.* **107**, 112001 (2011).
- [13] S. König, D. Lee, and H.-W. Hammer, *Annals Phys.* **327**, 1450 (2012), [arXiv:1109.4577 \[hep-lat\]](#).
- [14] S. Bour, S. König, D. Lee, H.-W. Hammer, and U.-G. Meißner, *Phys. Rev.* **84**, 091503 (2011), [arXiv:1107.1272 \[nucl-th\]](#).
- [15] Z. Davoudi and M. J. Savage, *Phys. Rev. D* **84**, 114502 (2011).
- [16] R. A. Briceño, Z. Davoudi, T. C. Luu, and M. J. Savage, [arXiv:1311.7686 \[hep-lat\]](#).
- [17] R. A. Briceño, Z. Davoudi, T. C. Luu, and M. J. Savage, *Phys. Rev. D* **88**, 114507 (2013).
- [18] D. Agadjanov, U.-G. Meißner, and A. Rusetsky, *JHEP* **01**, 103 (2014).
- [19] V. Bernard, M. Lage, U.-G. Meißner, and A. Rusetsky, *JHEP* **08**, 024 (2008).
- [20] M. Lage, U.-G. Meißner, and A. Rusetsky, *Phys. Lett. B* **681**, 439 (2009).
- [21] V. Bernard, M. Lage, U.-G. Meißner, and A. Rusetsky, *JHEP* **01**, 019 (2011).
- [22] M. Göckeler, R. Horsley, M. Lage, U.-G. Meißner, P. E. L. Rakow, A. Rusetsky, G. Schierholz, and J. M. Zanotti, *Phys. Rev. D* **86**, 094513 (2012).
- [23] N. Li and C. Liu, *Phys. Rev. D* **87**, 014502 (2013).
- [24] S. Kreuzer and H.-W. Hammer, *Eur. Phys. J. A* **43**, 229 (2010).
- [25] S. Kreuzer and H.-W. Hammer, *Phys. Lett. B* **694**, 424 (2011).
- [26] K. Polejaeva and A. Rusetsky, *Eur. Phys. J. A* **48**, 1 (2012).
- [27] R. A. Briceño and Z. Davoudi, *Phys. Rev. D* **87**, 094507 (2013).
- [28] U.-G. Meißner, G. Ríos, and A. Rusetsky, *Phys. Rev. Lett.* **114**, 091602 (2015).
- [29] P. Weisz, *Nucl. Phys. B* **212**, 1 (1983).
- [30] P. Weisz and R. Wohlert, *Nucl. Phys. B* **236**, 397 (1984).
- [31] M. Lüscher and P. Weisz, *Nucl. Phys. B* **240**, 349 (1984).
- [32] G. Curci, P. Menotti, and G. Paffuti, *Phys. Lett. B* **130**, 205 (1983).
- [33] H. W. Hamber and C. M. Wucur, *Phys. Lett. B* **133**, 351 (1983).
- [34] T. Eguchi and N. Kawamoto, *Nucl. Phys. B* **237**, 609 (1984).
- [35] B. Sheikholeslami and R. Wohlert, *Nucl. Phys. B* **259**, 572 (1985).
- [36] J. J. Dudek, R. G. Edwards, M. J. Peardon, D. G. Richards, and C. E. Thomas (for the Hadron Spectrum Collaboration), *Phys. Rev. Lett.* **103**, 262001 (2009).
- [37] J. J. Dudek, R. G. Edwards, M. J. Peardon, D. G. Richards, and C. E. Thomas (for the Hadron Spectrum Collaboration), *Phys. Rev. D* **82**, 034508 (2010).
- [38] R. G. Edwards, J. J. Dudek, D. G. Richards, and S. J. Wallace, *Phys. Rev. D* **84**, 074508 (2011).
- [39] S. Meinel, *Phys. Rev. D* **85**, 114510 (2012).
- [40] Z. Davoudi and M. J. Savage, *Phys. Rev. D* **86**, 054505 (2012).
- [41] R. Johnson, *Phys. Lett. B* **114**, 147 (1982).
- [42] B. Berg and A. Billoire, *Nucl. Phys. B* **221**, 109 (1983).
- [43] J. E. Mandula, G. Zweig, and J. Govaerts, *Nucl. Phys. B* **228**, 91 (1983).
- [44] B.-N. Lu, T. A. Lähde, D. Lee, and U.-G. Meißner, *Phys. Rev. D* **90**, 034507 (2014).
- [45] S. Altmann, *Math. Proc. Cambridge* **50**, 343 (1957).
- [46] I. Tanihata, H. Hamagaki, O. Hashimoto, Y. Shida, N. Yoshikawa, K. Sugimoto, O. Yamakawa, T. Kobayashi, and N. Takahashi, *Phys. Rev. Lett.* **55**, 2676 (1985).
- [47] J. Meng, H. Toki, S. Zhou, S. Zhang, W. Long, and L. Geng, *Progress in Particle and Nuclear Physics* **57**, 470 (2006).
- [48] A. Bohr, *Rev. Mod. Phys.* **48**, 365 (1976).
- [49] K. Rykhlinkaya and S. Fritzsche, *Computer Physics Communications* **174**, 903 (2006).